TISSUE ENGINEERING
Volume 7, Number 1, 2001
Mary Ann Liebert, Inc.

Evaluation of Metallic and Polymeric Biomaterial Surface Energy and Surface Roughness Characteristics for Directed Cell Adhesion

NADIM J. HALLAB, Ph.D.,[1] KIRK J. BUNDY, Ph.D.,[2] KIM O'CONNOR, Ph.D.,[3] RANDY L. MOSES, Ph.D.,[4] and JOSHUA J. JACOBS, M.D.[1]

ABSTRACT

Directed cell adhesion remains an important goal of implant and tissue engineering technology. In this study, surface energy and surface roughness were investigated to ascertain which of these properties show more overall influence on biomaterial–cell adhesion and colonization. Jet impingement was used to quantify cellular adhesion strength. Cellular proliferation and extracellular matrix secretion were used to characterize colonization of 3T3MC fibroblasts on: HS25 (a cobalt based implant alloy, ASTM F75), 316L stainless steel, Ti-6Al-4V (a titanium implant alloy), commercially pure tantalum (Ta), polytetrafluoroethylene (PTFE), silicone rubber (SR), and high-density polyethylene (HDPE). The metals exhibited a nearly five-fold greater adhesion strength than the polymeric materials tested. Generally, surface energy was proportional to cellular adhesion strength. Only polymeric materials demonstrated significant increased adhesion strength associated with increased surface roughness. Cellular adhesion on metals demonstrated a linear correlation with surface energy. Less than half as much cellular proliferation was detected on polymeric materials compared to the metals. However the polymers tested demonstrated greater than twice the amount of secreted extracellular matrix (ECM) proteins on a per cell basis than the metallic materials. Thus, surface energy may be a more important determinant of cell adhesion and proliferation, and may be more useful than surface roughness for directing cell adhesion and cell colonization onto engineered tissue scaffoldings.

INTRODUCTION

CURRENT TISSUE ENGINEERING TECHNOLOGIES to direct cell adhesion through surface-linked adhesion proteins, hydrogel layers, and surface treatments are approaching clinical use. However, quantitative relationships of how the underlying surface characteristics affect adhesion remain incomplete. Underlying surfaces may ultimately be exposed upon removal of surface treatment layers over the long term. There-

[1]Department of Orthopedic Surgery, Rush Presbyterian-St. Lukes Medical Center, Chicago, Illinois.
[2]Department of Biomedical Engineering, and [3]Department of Chemical Engineering, Tulane University, New Orleans, Louisiana.
[4]Department of Anatomy, Louisiana State University Medical School, New Orleans, Louisiana.

fore, it remains important to know the inherent cell adhesion properties of all implant materials including those with modified surfaces. Poor biomaterial performance is often caused by nonintegration of the implant with surrounding tissue or infection.[1] Post-operative tissue integration and infections are influenced by the relative ability of bacteria and autologous cells (*e.g.*, fibroblasts, osteoblasts, *etc.*) to adhere and colonize biomaterial surfaces. The ability to engineer directed cell responses to material surfaces is dependent upon a clear understanding of how different surface characteristics on various biomaterials affect implant–cell interactions. This understanding is prerequisite for optimizing scaffolding and implant surface performance.

Previously, we reported that an optimum range of surface charge was associated with maximal adhesion to metallic biomaterial surfaces.[2,3] In this investigation, we hypothesized that, similar to surface charge, an optimal range of surface energy and surface roughness may be associated with maximal cell adhesion and colonization on polymeric and metallic biomaterials. Cellular adhesion strength was determined by jet impingement.[2,4–6] Colonization characteristics of biomaterial surfaces were investigated by measuring cell proliferation as well as relative amounts and composition of the extracellular matrix (ECM) secreted by fibroblasts.

MATERIALS AND METHODS

Cell culture

3T3 Fibroblasts (BALB/c clone A31, American Type Culture Collection CCL 173) were cultured in Dulbecco's modified Eagle's medium (DMEM), and supplemented with 10% fetal bovine serum (FBS) and gentamicin, to form a subconfluent monolayer on the metals stainless steel (316L), cobalt-chromium alloy (HS25, F-75), titanium alloy (Ti-6Al-4V), and tantalum (Ta) and the nonmetals glass Corning™ tissue culture petri dishes, polytetrafluoroethylene (PTFE), silicone rubber (SR), and high-density-polyethylene (HDPE). All examples except glass petri dishes were obtained from Metal Samples Company (Munford, AL). All materials were seeded with an equal density of cells (approximately 10,000 cells/cm^2) and grown to near confluency over 2.5–3 days at 37°C and 95% humidity in 5% CO_2. The 3T3 fibroblast cell line was used between generations 5 and 10 (passages).

Jet impingement

When the cells were nearly confluent, the Petri dish containing the sample was transferred to a constant temperature bath at 37°C. A submerged laminar jet of 37°C phosphate-buffered saline (PBS, Gibco) solution (Reynolds no. $\approx$1750) was directed at the cells grown on the surfaces of the various materials to create a lesion in the cell layer. The jet issued from a nozzle oriented perpendicular to the cell layer, from a height of 2.514 mm (four times the nozzle diameter, 0.6285 mm). The cell layer was subjected to the flow for 30 s, a time period previously established Deshpande *et al.*[4] The shear stresses at the perimeter of the lesions created by the flow were determined according to the theory of Deshpande and Vaishnav.[4,5] Knowing the size of the lesion and using published nondimensionalized stress versus radial distance calibration curves,[5] the stresses required to erode the cells off the material surface were determined. Images of each lesion were digitally captured and processed to find T_s, the applied shear stress, at the perimeter of the lesion, according to methods previously described.[3] T_s is a quantitative measure of the shear strength with which cells adhere to surfaces.[2–5] Two glass petri dishes were used as controls in each measurement series to ensure the comparability of the data sets.

The lesions were detected under ultraviolet light after exposure to a solution of 5% fluorescein diacetate (Sigma Chemical Co.) in 70% acetone (Sigma Chemical Co.) mixed with phosphate-buffered saline (PBS) (Gibco) in the proportion of 5% stain to 95% saline.[2,3] Photographs of the lesions were taken and then digitized with an Abaton 2000 black and white scanner. The areas of the lesions were then calculated using NIH Image 1.51, image processing software.

Four lesions were created on each disk, one in each quadrant. The stress field for a given lesion rapidly decays with distance from the needle axis, *i.e.*, the stresses are negligible ($<$0.1% of max) beyond 3 cm from the nozzle which is an open area encompassed within a single quadrant. Thus, the flow to create a

given lesion did not affect the cells used in the adjacent areas where subsequent lesions were made. This procedure was repeated at least twice for each material, yielding a minimum of eight lesions for each material.

Surface roughness

Ti-6Al-4V specimens with three different surface roughnesses were studied. Roughness (R_a) was measured with a Tencor Alpha-Step 200 profilometer. The samples of the Ti alloy were identical in alloy content (obtained from the same stock). The three finishes used were: (1) as received (<100 grit), (2) 320 grit, and (3) 1.0-μm mirror alumina finish. Surface roughness (R_a) is defined as the average value of the distance from the surface to a center reference line.[3] The Tencor Alpha-Step 200 profilometer calculated an R_a value by summing the deviations from the centerline and dividing by the number of data points along a selected 80-μm length. Twenty-five points per micrometer were used, yielding a total of 2,000 data points for the determination of a single roughness value. Each sample was scanned in 25 randomly selected locations.

Surface energy

Total surface energy and the dispersive and polar components of surface energy for 316L, HS25, Ti-6Al-4V, Ta, glass, PTFE, and SR, were determined from contact angle measurements using six liquids on each material: PBS, glycerin, 30W-oil, DMEM, dimethylsulfoxide (DMSO), and benzene. The experimental procedures used for determination of solid/liquid/gas interfacial contact angles followed those of Andrade *et al.*[7] A series of eight drops (2 μL/drop) were placed on the samples, and the contact angle, θ, was measured using a digital camera (Connectix QuickCam™) connected to the eyepiece of an inspection zoom microscope (Bausch and Lomb StereoZoom 7). Images were acquired by a laptop computer (Apple, Duo 280) and θ determined using NIH Image image processing software, through measurement of the height and width of drops placed on the biomaterial surface. A series of at least eight drops were used in two trials, for a total of 16 contact angle measurements per liquid on a particular material surface.

To determine the components of polar (acid/base) and dispersion surface tensions of material surface A and liquid B according to the analysis of Schakenraad *et al.*,[8] the Young-Dupre equation:

$$\cos\theta = \frac{\gamma_{SV} - \gamma_{SL}}{\gamma_{LV}} \tag{1}$$

where θ, γ_{SV}, γ_{SL}, and γ_{LV} represent the contact angle, solid(S)/vapor(V), solid/liquid(L) and liquid/vapor surface energies, respectively, is combined with the interfacial energy (γ_{SL}) equation between any two surfaces. In the case of a solid surface and a liquid surface, (denoted S and L respectively) this relation is given by,

$$\gamma_{SL} = \gamma_S + \gamma_L - 2\sqrt{\gamma_S^d \gamma_L^d} - 2\sqrt{\gamma_S^{ab} \gamma_L^{ab}} \tag{2}$$

where d and ab represent the dispersion and polar (or acid/base) components of surfaces S and L. Combining equations (1) and (2) yields the following equation:

$$\cos\theta = -1 + \frac{2\sqrt{\gamma_S^d \gamma_L^d}}{\gamma_L} - \frac{2\sqrt{\gamma_S^{ab} \gamma_L^{ab}}}{\gamma_L} - \frac{\pi_e}{\gamma_L} \tag{3}$$

where π_e is the spreading pressure, defined as $\gamma_S - \gamma_{SV}$, the difference between the solid and solid–vapor surface energies, respectively.

Performing contact angle measurements with liquids whose surface energy components γ_L^{ab} and γ_L^d are known enables the calculation of γ_S^{ab} and γ_S^d, according to the following procedure. In equation 3, the known parameters are the dispersion component, γ_L^d, the polar component γ_L^{ab}, the total surface energy of the liquid γ_L, (equal to $\gamma_L^d + \gamma_L^{ab}$) and the measured contact angle θ. Dispersion surface tension of the liquids was obtained by contact angle measurement on Parafilm, a purely nonpolar surface of known surface energy (*i.e.*, $\gamma_S^{ab} = 0$ and $\gamma_S^d = 29.9$ ergs/cm^2)[8] where equation (3) becomes

$$\cos\theta = -1 + 2\,\frac{\sqrt{\gamma_S^d \gamma_L^d}}{\gamma_L} \tag{4}$$

Then the polar components of the liquids surface tension could be calculated (total = $\gamma_L^d + \gamma_L^{ab}$).

A linear approximation between spreading pressure and the surface energy of the various liquid was used: $\pi_e = C_1(\gamma_L) + C_2$. Constants C_1 and C_2 represent two additional unknown constants to be determined, following a procedure previously established.[8] A least squares procedure (Mathematica™, Wolfram Research) was used to approximate the values of the four unknowns γ_S^{ab}, γ_S^d, C_1, and C_2 that best fit the seven equations of form (3) corresponding to the contact angles for the seven liquids measured on each biomaterial surface.

ECM protein analysis

ECM from fibroblasts grown on samples of HS25, Ti-6Al-4V, Ta, 316L, glass, SR, and PTFE was analyzed. To separate the cells from the ECM, a calcium-specific chelating agent was used, EGTA (ethylene glycol-*bis*(*b*-aminoethyl ether),*N*,*N*,*N*′,*N*′-tetraacetic acid), (Sigma Chemical Co.). To preserve the ECM from degradation by enzymes, a cocktail of proteolytic inhibitors was used that contained 0.5 μg/mL leupeptin (Sigma, St. Louis, MO), 1 μg/mL peptstatin (Sigma Chemical Co.), and 1 nM phenylmethylsulfonyl fluoride (PMSF; Sigma, St. Louis, MO). Cells were eluted in a 4°C environment while gently agitated rotationally at a speed of 30–40 rpm. The cells were confirmed to be detached after approximately 48 h using an optical light microscope. After the removal of the fibroblasts, the surfaces of the materials were rinsed twice with 20 mL of PBS. A 0.25% trypsin-PBS solution was used after treatment with EGTA to cleave disulfide bonds holding any residual cells to the petri dish. Cell counting techniques were used to verify that all cells were previously removed from the ECM with EGTA.

After removal of cells from the ECM, a 2% sodium dodecyl sulfate (SDS) solution was used to elute the extracellular matrix proteins.[2,3,9] SDS–protein solutions were then concentrated using microfiltration tubes (Centricon-3, Amicon, Beverly, MA).

The elutant from each sample was examined with one-dimensional polyacrylamide gel electrophoresis (SDS-PAGE, BioRad) using a medium range molecular weight gel (12.5%, 14–200 kDa). Between 20 and 100 μL of elutant from each material surface were loaded into the gel lanes, as was 4 μL of calibration marker (HMW Calibration Kit 17-0446-01, Pharmacia) and 4 μL of serum protein diluted to a ratio of 1% serum in 2% SDS. For a given run, the same amount of elutant was used for each material. Visualization of the protein was performed by staining the gels with silver nitrate (Sigma Chemical Co.). The gels were photographed, digitized (using procedures previously described for jet impingement), and then analyzed using NIH Image 1.51. Image enhancement techniques were limited to background subtraction.

The total protein adsorbed on each sample was approximately determined using molecular markers (HMW Calibration Kit 17-0446-01, Pharmacia). The known amount of each marker protein was used to calculate a conversion factor between the degree of gel darkening caused by the silver stain and the amount of protein. The chemical technique of silver staining has been shown for most proteins to be linear with protein quantity over a 40-fold range. This corresponds to 0.005 to 0.2 μg/cm^2 of protein on the electrophoresis gels to be developed. At concentrations of protein greater than 0.2 μg/cm^2, saturation begins to occur, resulting in a nonproportional darkening effect of the silver staining. In this investigation, however, unsaturated gels were used to estimate the total amount of protein adsorbed on a particular sample by summing all the stained protein bands on the electrophoresis gel lane associated with that sample. Such estimates were then averaged for all measurements with each material. This mean was then converted to the area of concentration on the biomaterials by multiplying by the ratio of the elutant volume from the material to the volume employed in the electrophoresis measurement.

Densitometry profile plots were constructed from scanned digital images of the gels (HP ScanJet 4c, Hewlett Packard). Image processing using NIH Image was limited to background subtraction (one pass). Twenty-five repeatable, identifiable peaks on all the gels were used to compare differences (if any) in observed proteins on the various material surfaces on five repeated ECM-electrophoresis gel measurements for each of the materials tested.

The delineation between passively adsorbed serum proteins and actively secreted ECM proteins was de-

termined using previously obtained results[2] of passive serum adsorption on the same material samples. These previous results[2] were determined using the identical methodology as described above, *i.e.*, elution using 2% SDS and examination using one-dimensional SDS-PAGE, 12.5% gel for all the material samples (Ti not reported). In this previous investigation,[2] differential passive serum protein adsorption (Vroman) characteristics over time were examined on 316L, HS25, Ta, glass, PTFE, and SR material samples. Therefore, a steady-state adsorption pattern of serum proteins was previously determined and used to correct total protein (measured in the present investigation) to secreted ECM protein. However, similar compositional and bulk amounts of passively adsorbed serum protein were found on these different surfaces.[2]

Cellular proliferation on the different biomaterials was determined using trypan-blue staining and hemacytometry. Cells were collected from each of the biomaterials at the time of ECM analysis (3 days).

Electron microscopy

TEM observation (using a Philips CM10 transmission electron microscope, Frankfurt, Germany) was performed on fibroblasts grown on Ti-6Al-4V, 316L, tissue culture polystyrene (TCPS), and SR to see cross sections of the cells transverse to the material surface. Detecting cell cross sections under TEM was accomplished by embedding the cells in epoxy resin.[11] The metal/epoxy samples were sequentially treated with acid solutions to dissolve the metal for sample sectioning as follows: 1 h exposure to a solution of 7% nitric acid (HNO_3) and 27% hydrofluoric acid (HF) followed by a 2- to 3-h exposure to 22% hydrochloric acid (HCl) and 10% HNO_3. Less than a 2°C temperature rise was observed during dissolution, preventing thermal degradation of embedded cells.

Statistics

Measured data were subjected to statistical analysis using Student's *t*-tests. Student's *t*-tests for independent samples with unequal or equal variances were used to test equality of the mean values at a 95% confidence interval ($p < 0.05$). All cell adhesion measurements were predetermined to be normally distributed for each material.

RESULTS

Surface energy

The dispersion and polar surface tension components of the liquids used to obtain the components of surface energy of the different materials are shown in Table 1 as is the fractional polarity (FP): $\gamma_{ab}/(\gamma_{ab} + \gamma_d)$ of these liquids. The contact angles for each of the liquids on each of the test materials are listed in Table

Table 1. Tabulated Values of Total, Polar, and Dispersion Surface Energy Components of Liquids, Obtained from Contact Angles upon a Purely Dispersive Surface (Parafilm) or Obtained from Published Values

	Components of surface energy			
Liquid	*Dispersion* γ^d *(ergs/cm²)*	*Polar (acid-base)* γ^{ab} *(ergs/cm²)*	*Total* $\gamma^d + \gamma^{ab}$ *(ergs/cm²)*	*Fractional polarity* $\gamma^{ab}/(\gamma^d + \gamma^{ab})$
Glycerin	26.1	39.4	65.5	0.60
30-Oil	28.6	3.0	31.6	0.09
PBS	22.0	35.2	57.2	0.62
Media	20.2	30.9	51.1	0.60
DMSO[a]	34.9	8.6	43.5	0.20
Benzene	28.5	0.6	29.2	0.02

[a]Published value.[7]

Table 2. Average Contact Angle (θ) in Degrees for Various Liquids on Biomaterial Samples

Liquid	*SR*	*PTFE*	*Glass*	*Ta*	*Ti*	*316L*	*HS25*
Glycerin	106.3 ± 3.1	120.3 ± 5.2	46.2 ± 8.3	66.5 ± 3.4	50.0 ± 2.9	55.2 ± 2.3	83.0 ± 1.4
30-Oil	49.4 ± 0.9	56.3 ± 1.8	19.7 ± 4.4	8.0 ± 1.7	10.6 ± 0.9	6.5 ± 1.8	14.3 ± 1.6
PBS	115.3 ± 3.6	122.9 ± 2.8	59.7 ± 9.6	44.3 ± 3.6	51.0 ± 4.7	60.0 ± 8.9	63.2 ± 3.1
DMEM	106.0 ± 5.1	120.0 ± 5.5	44.8 ± 5.4	51 ± 7.3	46.4 ± 3.7	59.3 ± 2.5	69.0 ± 1.1
DMSO	86.3 ± 2.7	95.4 ± 1.3	38.8 ± 3.9	42.3 ± 8.3	28.0 ± 3.8	50.3 ± 4.6	65.4 ± 2.3
Benzene	23.5 ± 3.2	36.5 ± 5.6	9.8 ± 1.4	2.4 ± 0.2	7.0 ± 0.6	7.8 ± 1.2	10.4 ± 2.3

2. As expected, the contact angles are generally larger for the low-energy, hydrophobic polymers (SR and PTFE) than for the higher energy, more hydrophilic materials (glass, Ta, Ti-6Al-4V, 316L, and HS25).

The total surface energy (the dispersion plus the polar component) and the fractional polarity of the materials used for cellular adhesion strength measurements are shown in Table 3, with their corresponding adhesion strength values. Materials of higher surface energy have higher cellular adhesion (Fig. 1). The polar, dispersive, and total surface energy components of each material are shown connected by horizontal lines. The highest correlation occurs between the total surface energy and cellular adhesion strength (Pearson's correlation coefficient = 0.92, $R^2 = 0.93$). The correlation is similar for the polar component (Pearson's correlation coefficient = 0.91, $R^2 = 0.91$). However, less correlation was observed between the dispersion component and adhesion strength (Pearson's correlation coefficient = 0.79, $R^2 = 0.63$).

Surface roughness

The influence of surface roughness on the associated adhesion strength is shown in Fig. 2. Overall there is no clear effect of surface roughness (independent of material type) on the cellular adhesion strength. However, if the materials are separated on the basis of material class (*i.e.*, polymer vs. nonpolymer), a pattern seems to emerge.

The adhesion strength for both of these material classes seems to vary logarithmically with surface roughness (Pearson's correlation coefficient = 0.82 non-polymeric and 0.98 polymeric with R^2 values of 0.73 non-polymeric and 0.97 polymeric). The results for the nonpolymeric materials are likely confounded by the presence of a maximum limit of adhesion strength (T_s), which may be associated with cell cohesion strength, an effect considered in more detail later.

Table 3. Dispersion and Polar Surface Energy Components, Total Surface Energy, Fractional Polarity, and Corresponding Cellular Adhesion Strength of Various Biomaterials

Material	*Dispersion component* γ^d *(ergs/cm²)*	*Polar (acid/base) component* γ^{ab} *(ergs/cm²)*	*Total surface energy* $\gamma^{ab} + \gamma^d$ *(ergs/cm²)*	*Fractional polarity* $\gamma^{ab}/(\gamma^{ab} + \gamma^d)$	*Cellular adhesion strength,* T_s *(dynes/cm²)*
HS25	64.80	80.80	121.10	0.667	472.50
316L	33.40	96.24	129.65	0.741	458.80
Ta	40.06	60.53	100.59	0.602	407.10
Ti	38.53	79.96	118.49	0.675	278.00
Gl	24.79	45.00	69.78	0.645	254.00
PTFE	16.86	0.09	16.95	0.005	101.40
SR	20.82	0.07	20.89	0.003	31.72

Note: Standard deviations for the polar and dispersion terms are not available, due to the determination of these terms through least squares fitting of equation 3.

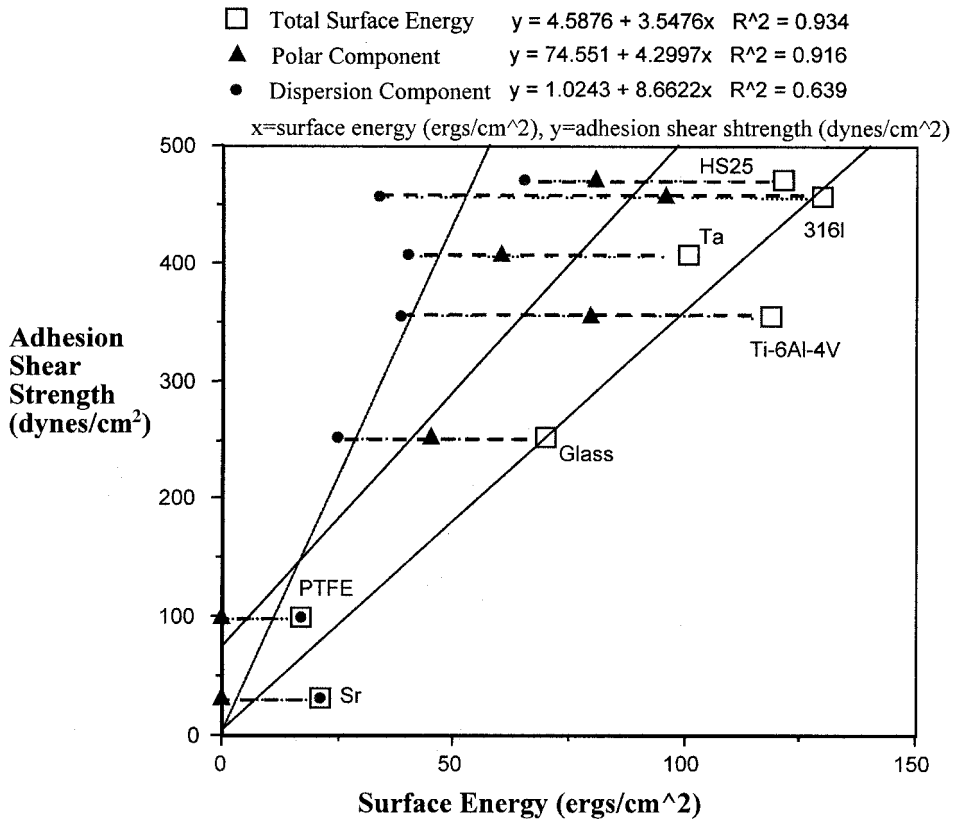

FIG. 1. Total surface energy and components for different materials related to the corresponding cellular adhesion shear strength. Note: Dotted lines connect total surface energy and its components for each material.

The variation of fibroblast adhesion strength with roughness of Ti-6Al-4V is shown in Table 4. The adhesion shear strengths of these three surfaces were not statistically distinct from one another. These results were generated from two trials in which six lesions were produced on each of the three titanium samples.

Cell colonization

The average total number of cells per unit area is shown in Fig. 3 for the various materials employed in the ECM study. There were approximately five to six times as many cells on the metallic materials (Ta, Ti, 316L, and HS25) and glass than observed on the polymeric materials (SR and PTFE). The difference between any nonpolymer and any polymer was found to be statistically significant ($p < 0.05$).

ECM biofilm

ECM proteins eluted from the surfaces of the biomaterial samples were analyzed using the SDS-PAGE techniques previously described. Figure 4 shows a captured digital image of a typical PAGE gel. Some ECM proteins were observed on the metallic surfaces, which were not apparent on the polymeric materials. The most prominent of these ECM proteins are labeled 1 to 5 in Fig. 4, and correspond to molecular weights of approximately 310, 247, 82, 72, and 50 kDa, respectively.

The total amount and composition of ECM proteins found on the metallic surfaces were approximately the same as those on the polymeric surfaces. However, when ECM protein (either in total or categorized by molecular weight range) was corrected for passively adsorbed serum protein and divided by the number of cells detected on each surface, an obvious difference emerged between the two material classes. A greater amount of total and secreted ECM, on a per-cell basis, was apparent on materials of low adhesion

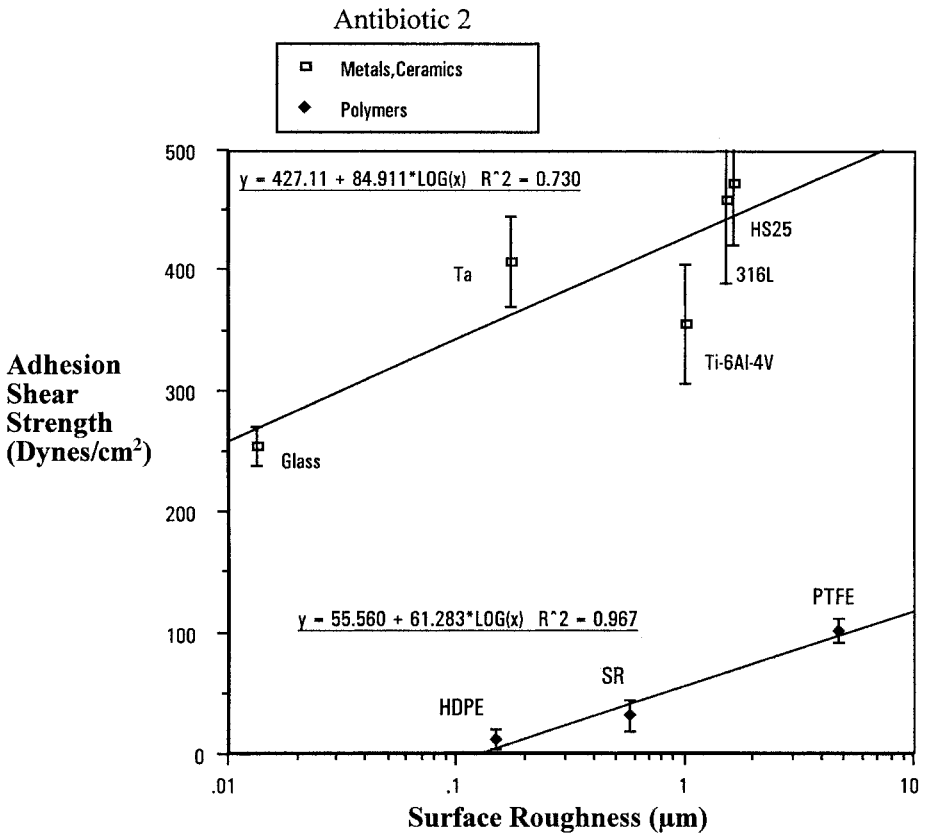

FIG. 2. Surface roughness (*x* axis) versus cellular adhesion shear strength (*y* axis) relationships for higher adhesion, higher surface energy metals, and ceramics compared to lower surface energy polymers. *R* is the correlation coefficient. Note: Error bars indicate standard deviations.

(SR and PTFE) when compared to the metallic materials (see Fig. 5). These total ECM differences between any nonpolymer and any polymer were determined to be statistically significant ($p < 0.1$). Glass, a material of intermediate adherence, showed the smallest amount of ECM on per cell basis.

The concentrations in μg/cell of total ECM proteins within specific molecular weight ranges for each of the materials tested are shown in Fig. 6. The greatest differences between the two classes of material lie in the 127–310 kDa and 50–71 kDa ranges. Molecular weight proteins of 247–221 and 68–55 kDa showed significant differences ($p < 0.05$) between the materials of high-adhesion (glass and the metals) and the low-adhesion polymers.

TABLE 4. FIBROBLAST SHEAR STRENGTH ON TI ALLOY SAMPLES DIFFERING IN SURFACE ROUGHNESS

Material	*Surface finish*	*Surface roughness (μm)*	*Adhesion shear strength (dynes/cm^2)*	*Standard deviation (dynes/cm^2)*
Ti-6A1-4V	milled	1.019	355	50
	320 grit	0.123	416	60
	1.0 μm	0.0249	429	27

Note: Results are averaged from 12 total lesions (four lesions/sample, for three trials of each roughness sample).

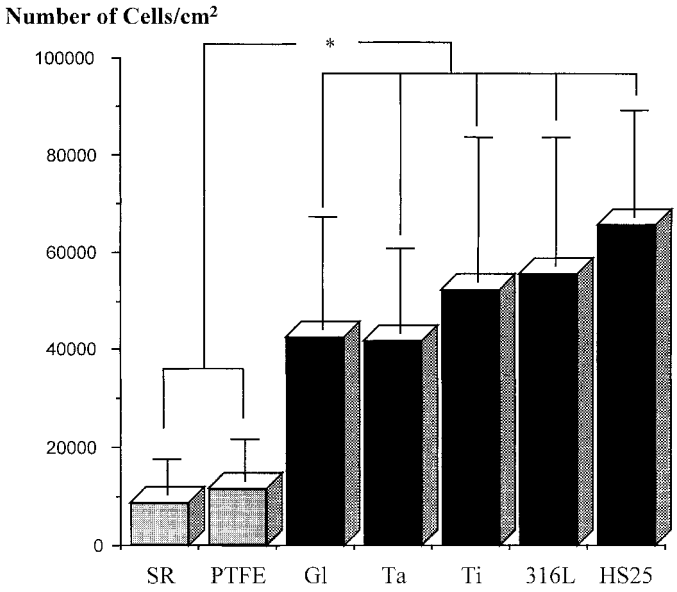

FIG. 3. Cellular density after 3 days of growth on various substrate materials. Note: All materials were seeded with an equal concentration of approximately 1–6 $\times$ 10^4 cells/cm^2. Error bars indicate standard deviations and "$*$" indicates statistically significant differences (Student's t-test, $p < 0.05$), between any nonpolymer to any polymer.

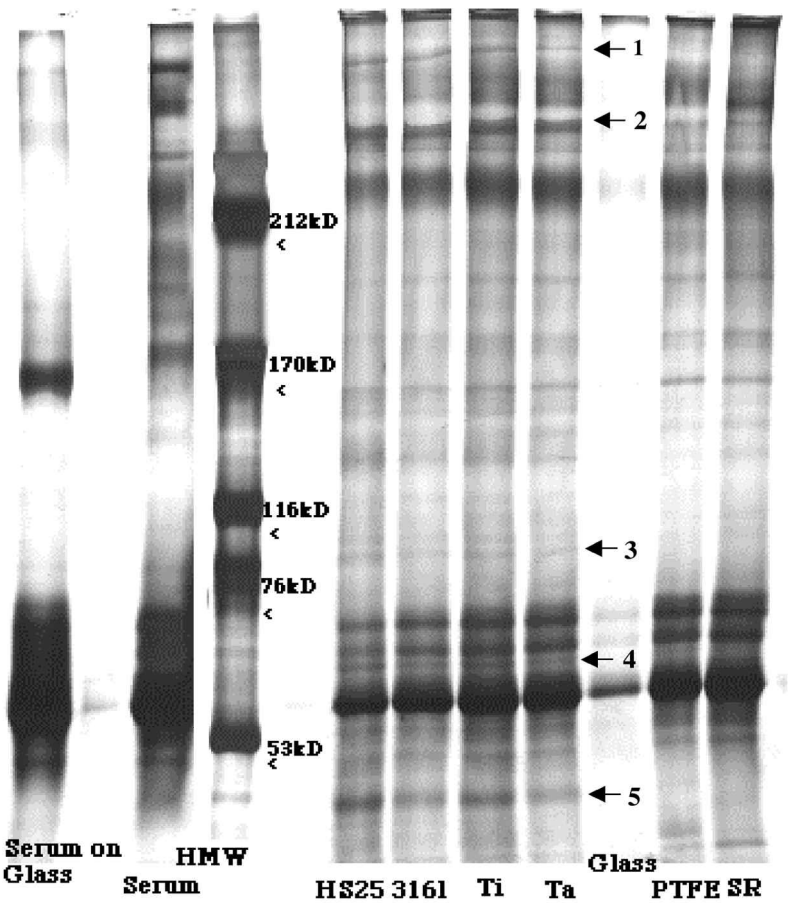

FIG. 4. Gels showing a typical pattern of secreted ECM and adsorbed serum proteins eluted from the surface of different biomaterials after the removal of the cellular monolayer. Note: High-molecular-weight proteins are at the top of the figure and those of low-molecular-weight are at the bottom. "HMW" indicates the high-molecular-weight standards, "serum on glass" indicates adsorbed serum proteins on glass, and "serum" indicates proteins present in the serum used to supplement the media.

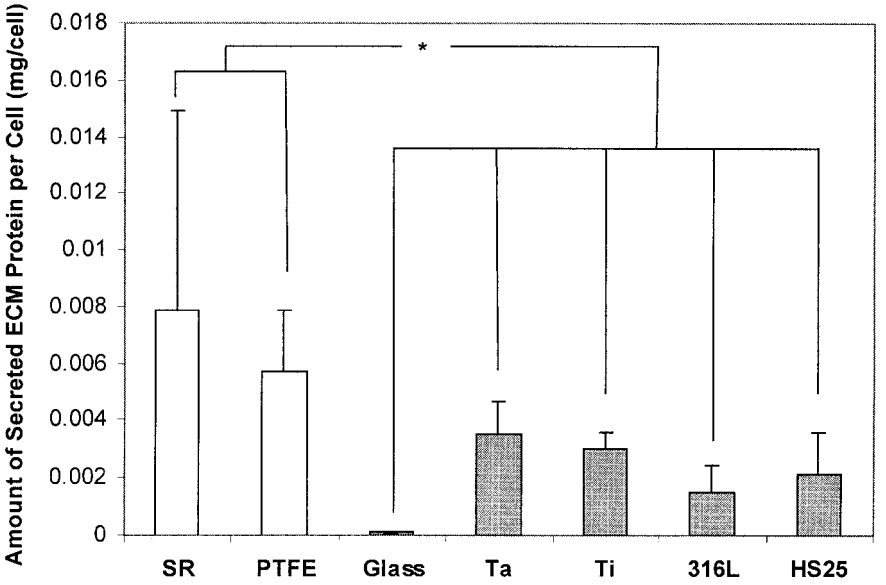

FIG. 5. Total amount of secreted ECM protein, on a per cell basis, eluted from various material surfaces. Note: Error bars indicate standard deviations and "*" indicates statistically significant differences (Student's *t*-test, $p < 0.1$), between any nonpolymer to any polymer.

Cell–biomaterial interfacial morphology

TEM micrographs of transversely cut sections of fibroblasts, grown on Ti-6Al-4V and silicone rubber (Fig. 7) typify cell behavior on the two materials. The bottom-most electron dense line in Fig. 7, indicated by arrows, represents the substrate surface. The gap between the line identifying the material surface and the ventral membrane of the cell is larger on the low-adhesion SR than on the high-adhesion Ti-6Al-4V. Two focal adhesions can be seen in Fig. 7A, directly above the tips of the arrows, identified by the dark areas of contact between the cell membrane and the surface of the material. There are no focal contacts between the cell and the SR surface. Focal contacts upon SR were difficult to locate because of the low density of cells on this material and because the transverse sections used were unlikely to "cut" through the relatively few focal contacts connecting the cells to the substrate.

DISCUSSION

The surface energy of a material can be affected by several surface characteristics, such as chemical composition, surface charge, and microstructural topography. However, the relationships between these surface properties are not always clear; *e.g.*, in some circumstances, wide variations in surface charge produce only small changes in surface energy.[7]

Of the two surface energy components, shown in Fig. 1, the polar component, γ_{ab}, seems to be the most accurate determinant of cellular adhesion strength. Dispersion component, γ_d, was relatively the same ($<10\%$ variation) for all materials, thereby suggesting a causal relationship of polar surface energy on cellular adhesion strength. Surface energy parameters did not directly demonstrate an optimal range of adhesion strength as initially hypothesized. Instead, a proportional increase of adhesion strength with surface energy was observed. An optimal range of adhesion strength in terms of surface energy characteristics can be observed indirectly using fractional polarity values.

Fractional polarity, $\gamma_{ab}/(\gamma_{ab} + \gamma_d)$, which has been previously correlated with cell spreading and cell growth (defined by some as measures of cellular adhesion),[8,12,13] demonstrated a roughly parabolic relationship with cellular adhesion strength (see Fig. 9). However this correlation remains a relatively weak

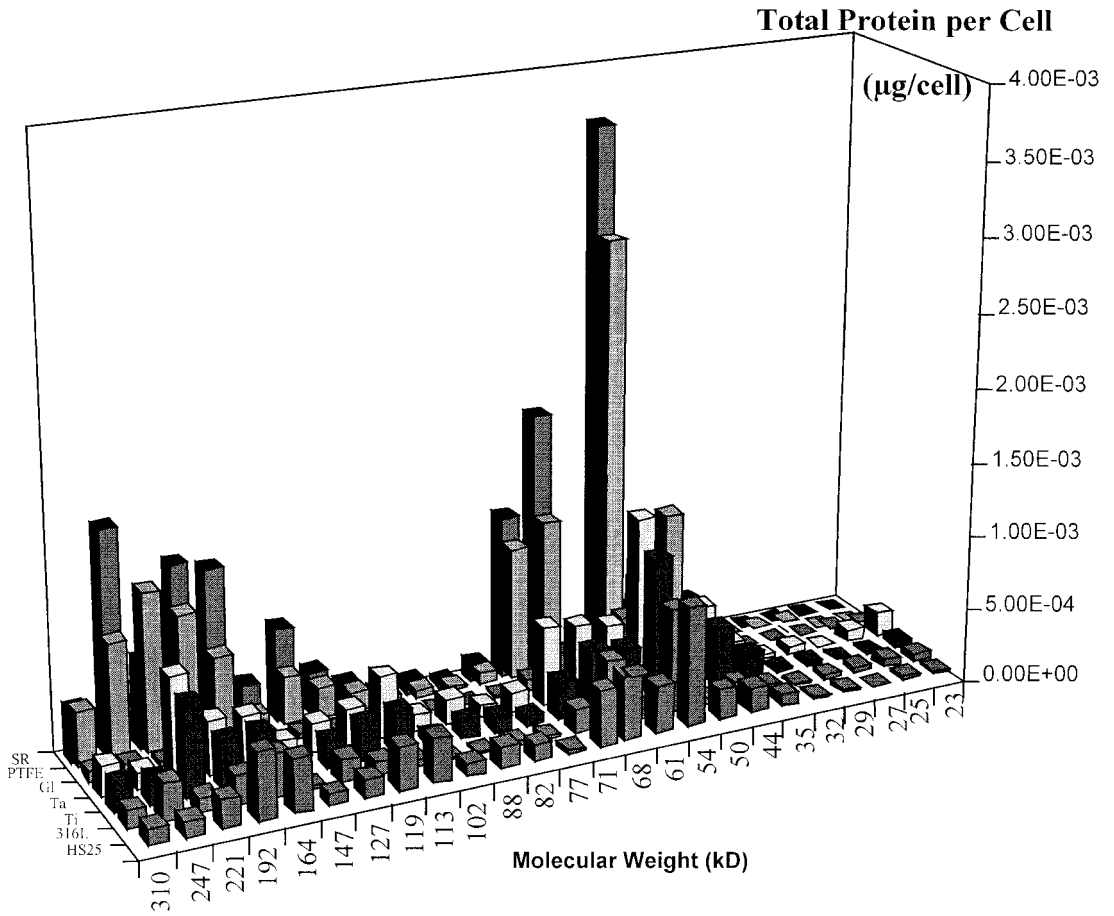

FIG. 6. The amount of ECM proteins secreted and adsorbed per cell for different materials.

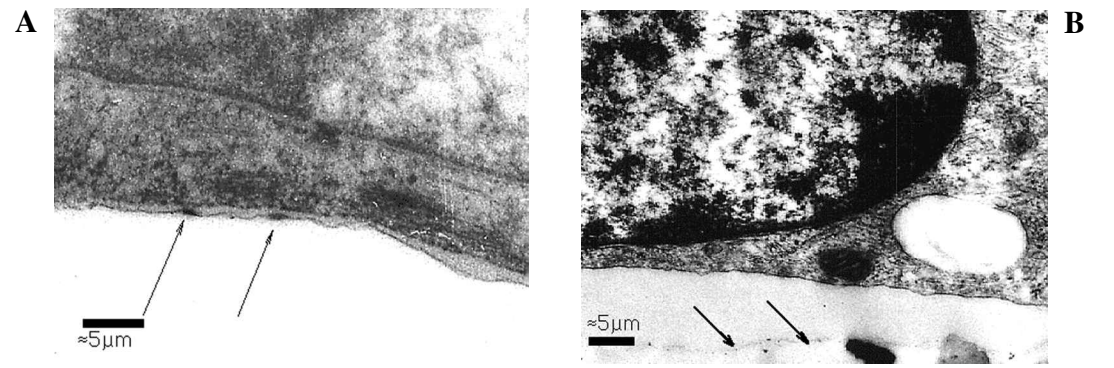

FIG. 7. Transmission electron micrograph of 3T3 fibroblasts grown on Ti-6Al-4V (**A**) and silicone rubber (**B**) of equal surface roughness (original $R_a = 1$ μm). Note: There is close proximity of the cell to the electron dense line representing the original Ti-6Al-4V growth surface (and focal contacts indicated by arrows) and the relatively wide gap between the cell-SR growth surface.

($R^2 = 0.785$) approximation despite the use of additional fractional polarity data culled from the literature[8,13,14] and included in the graph of Fig. 9 (*i.e.*, PTFE, SR, HDPE, Tissue Culture Polystyrene, and Glass).

Cellular adhesion may be influenced by variations in surface roughness (see Fig. 2). However, without categorization into two classes of high and low surface energy materials, the resulting scatter of data shows no surface roughness dependency. Once divided into two classes of materials of high and low surface energy, they seem to vary proportionally with surface roughness. While this proportional relationship for high surface energy materials shows moderate correlation (Pearson's coefficient = 0.82), the values themselves were not statistically distinct ($p < 0.1$) from one another. The polymers tested demonstrated statistically significant differences in adhesion strength between one another ($p < 0.05$).

This statistical indifference associated with high levels of cellular adhesion strength on various high-energy metallic materials is consistent with previous reports of membrane–substrate (*i.e.*, cell to metal) strength exceeding the cohesive strength of the cell membrane itself during jet impingement testing.[16–20] Richards *et al.* used high-resolution SEM to observe that during jet impingement, metallic (high-energy) surfaces caused fibroblast cell membranes to rupture before cell–substrate connections were broken.[16,17] If a similar phenomena occurs in the present investigation, then the cellular cohesive shear strength is approximated as 350–400 dynes/cm^2. This is lower than previously reported cohesion values (approximately 3,000 dynes/cm^2) for human ACL fibroblasts.[15] However, this variation in cohesion strength is possibly due to differences in cell type, culture environment, or testing technique.

Our findings suggest that the influence of surface roughness upon cell adhesion strength may be secondary to surface energy on high energy (*i.e.*, metallic) substrates. This is consistent with findings by Bundy *et al.*,[19,20] where no obvious relationship between *in vitro* cellular adhesion strength and surface roughness was detected between samples of milled, 80 grit, 400 grit, 1,000 grit, and 1-μm diamond-polished 316L stainless steel, where it was also likely the binding strength of integrins and/or adhesion proteins to the material surface (or biofilm) and the membrane exceeded the cohesive strength of the cell membrane.

Likewise, in this investigation, statistically indistinct cellular adhesion strengths were found for three surface roughness values of Ti-6Al-4V (see Table 4). These results support the hypothesis that surface roughness is likely a secondary and relatively noninfluential effect compared to the surface energy present on metallic materials. In general, a complex relationship between surface roughness and surface energy may exist where surface roughness exacts more influence over cellular adhesion strength on low surface energy materials (polymers). This influence of surface roughness may decrease as surface energy increases until it exceeds roughness in mediating adhesion and then continues exert more dominance until a point is reached where cell adhesion to a surface exceeds that of cell cohesion. This is schematically represented in Fig. 8.

The lack of any clear relationship between cellular adhesion strength and surface roughness, (for metallic biomaterials) as tested by jet impingement on a cell monolayer *in vitro* does not necessarily negate the use of surface roughness as a strategy for increasing tissue adhesion to metallic implant surfaces *in vivo*. Geometrical (surface roughness) variation, while indicated as an ineffectual mediator of adhesion at the microscopic level of cellular attachment, may provide an effective interlocking mechanism with tissue at a more macroscopic level. This hypothesis is supported by earlier studies conducted by Bundy *et al.*,[21] which indicated that increased surface roughness resulted in greater tissue adhesion as determined by peel tests on Ti-6Al-4V and 316L samples subcutaneously implanted in mice.

Given that cell adhesion and cell colonization are intimately related and that adhesive surfaces foster colonization, it is likely that techniques for manipulating cell–biomaterial interfaces will include the manipulation or judicious choice of substrate materials with appropriate surface energy and surface roughness characteristics. Therefore, increasing the roughness of low-energy surfaces for directing increases in microscopic cellular attachment is likely a more practical strategy for polymeric surfaces than metallic surfaces. Regulating surface charge or surface energy (*i.e.*, through judicious use of alloy composition, surface treatment, imposed potential, *etc.*) may be more effective strategies for manipulating cellular adhesion (up or down) to metallic biomaterials.

It is difficult to ascertain whether the differences in adhesion strengths are related to the cell's ability to secrete appropriate adhesion proteins or whether proteins at the material interface are less able to gain a strong foothold. Classically the concern has centered on the biofilm of the material interface. The vastly different adhesion strengths between the low and high surface energy materials are exemplified in the mi-

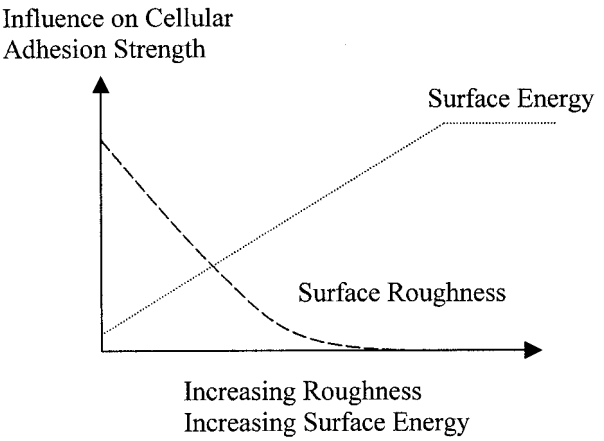

FIG. 8. Proposed schematic relationship between surface roughness, surface energy, and their respective influence on cellular adhesion strength.

crographs of Fig. 7, where differences in cell attachment show a relatively large gap and relatively sparse focal contacts between the cell surface and the substrate of a polymeric material (SR) when compared to a metallic material (Ti-6Al-4V) of equal surface roughness. Limitations associated with the number of micrographs taken and the difficulty associated with detecting any focal contacts on transverse sections of SR prohibited quantification of focal contact frequency. However, it seems that unless sufficient and/or effective focal adhesions are formed, the surfaces involved will not be as "cell friendly." How mechanistically surfaces mediate this formation remains relatively uncharacterized. Although speculative, one hypothesis is that biomaterial surface energetics affect both the ability of these cells to form focal adhesions and the efficiency with which focal adhesion proteins can bind to the surface. This hypothesis is consistent with observations of the relatively repulsive effect of the low energy surfaces (*e.g.*, SR) on the basolateral cell membrane (Fig. 7) and observations of differential ECM levels presumably secreted for attachment purposes.

The evaluation of bulk differences in ECM proteins produced by fibroblasts on different materials revealed that greater amounts of ECM protein were produced on materials of low adhesion and low surface energy. ECM proteins that appear to be more prominent on polymers (low adhesion materials) than metals on a per cell basis, range from 311 to 50 kDa in molecular weight (Fig. 6). Additionally, the proteins identified in Fig. 4 as apparent on metallic materials and not on polymers (of molecular weights 330, 247, 82, 72, and 50 kDa) might play an important role in the molecular linkage at the cell membrane (*e.g.*, RGD sequence) or the material substrate. Cell adhesion molecules that might correspond to some of these peaks are collagen type I or III (300 kDa), fibronectin (220 kDa), and vitronectin (77 kDa).[22] However, the determination of which ECM proteins these are would require further analysis using more sophisticated protein separation techniques, such as two-dimensional electrophoresis, radiolabeling, and, ultimately, protein sequencing.

The total ECM proteins are comprised of both passively adsorbed serum proteins (from supplemented medium) and cell-secreted proteins. Figure 10 shows the amount of total ECM, both including and excluding the relatively constant contribution of passively adsorbed proteins where, except for glass, the majority of eluted protein came from cell synthesis. This illustrates the small likelihood that passively adsorbed serum protein(s) from the culture medium play a dominant role in the ultimate determination of cell adhesion behavior on such widely variant materials. Interestingly, glass, with such an anomalous relationship between secreted ECM/cell and cell adhesion, may be a poor substrate on which to study cell adhesion behavior for extrapolation to metallic and polymeric implant materials.

A comparison of the secreted ECM protein (shown in Fig. 5) seems to imply that increased ECM protein production per cell is associated with biomaterials of decreased cellular adhesion strength. Likewise, when ECM secretion per cell is matched with the corresponding total surface energy, the resulting pattern

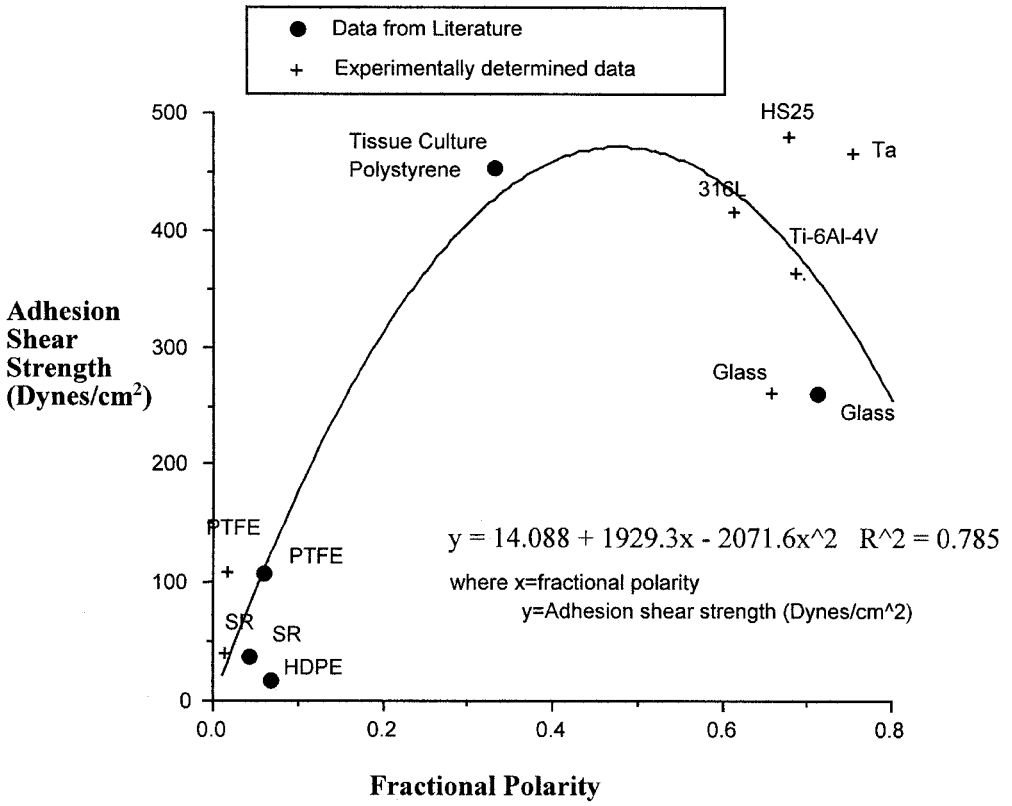

FIG. 9. Cellular adhesion shear strength variation with fractional polarity (obtained from experimental and literature-culled data). Note: Experimentally determined data is indicated by a "+". Data culled from the literature (Schakenraad *et al.*, 1986; Bagnall *et al.*, 1980; VanDiijk *et al.*, 1988) is represented by a "●".

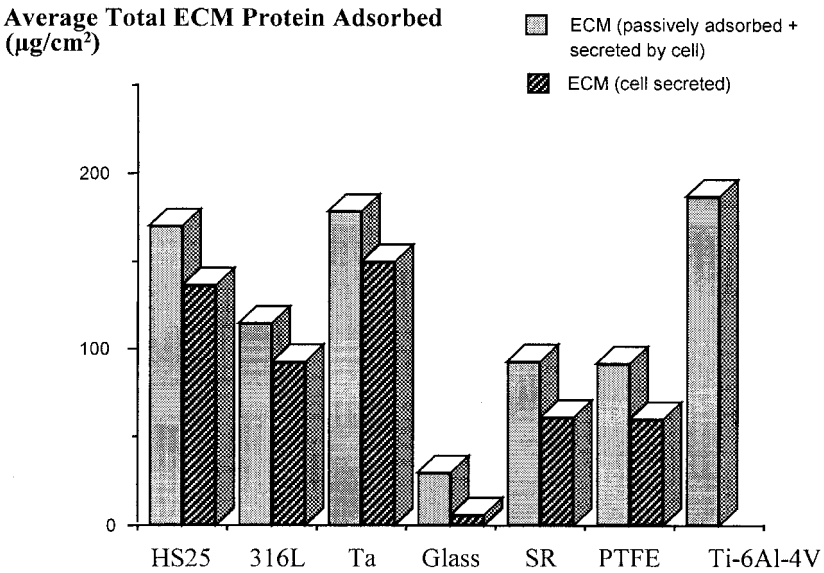

FIG. 10. Total amount adsorbed ECM protein resulting from both cell synthesis and passive adsorption (secreted + adsorbed), compared to the amount secreted.

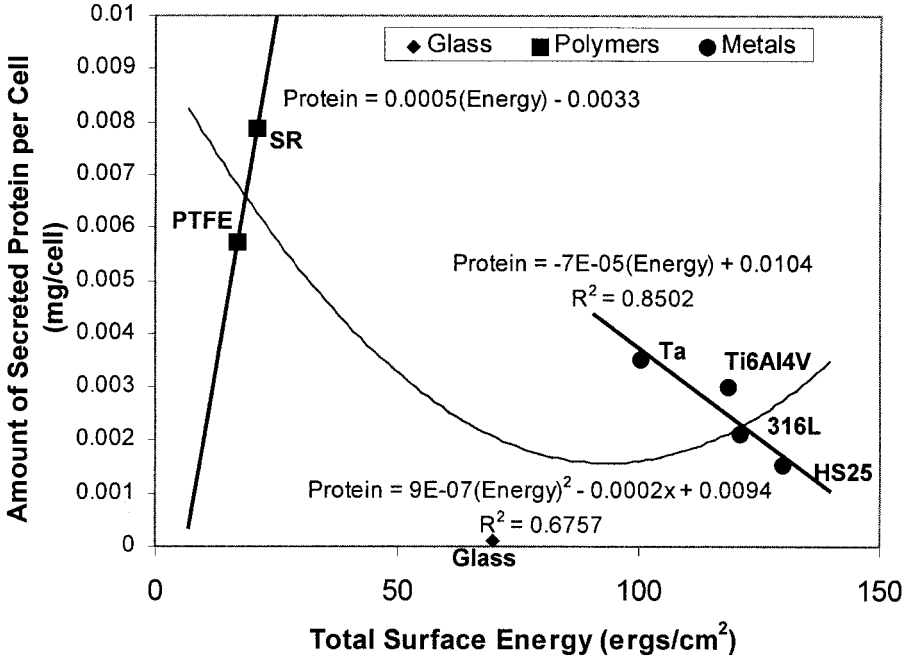

FIG. 11. The variation of ECM protein deposition per cell on materials of different total surface energy. Note: Parabolic regression applies to all data.

demonstrates a general decrease in the amount of secreted ECM associated with an increase in surface energy (*i.e.*, the parabolic regression in Fig. 11). However, when grouped separately, metallic and polymeric materials seem to behave differently (*i.e.*, linear regression lines in Fig. 11). Although there are two fee data points within each group to characterize intergroup trends conclusively, polymeric materials seem to demonstrate an increase in ECM associated with increasing surface energy whereas the opposite is true for the metallic materials. Although two polymeric material data points are insufficient to base any assertion of ECM protein versus polymer surface energy relationship, the four metallic materials tested more convincingly indicate a relatively linear inverse relationship between secreted ECM and total surface energy (Fig. 11). Why mechanistically this increase in ECM production is associated with a decrease in surface energy both generally (all materials tested) and among metallic biomaterials remains unknown. However, if differential ECM production is causally related to cell adhesion, likely explanations include: (1) that these cells attempt to adhere to "hostile" surfaces by producing greater amounts of adhesion related proteins but these proteins are then unable to form suitable attachments to the surface (or biofilm), or (2) that critical adhesion protein(s) exist in greater amounts on highly adhesive surfaces but at concentrations low enough to render one-dimensional electrophoresis analysis ineffective on a per cell basis. Although speculative, this increase in ECM protein secretion may help explain why cells relatively retain phenotypic expression upon highly adhesive surfaces, given there is less diversion from normal cell function. Further studies involving specific labeling of adhesion proteins both spatially and functionally could help to clarify whether differential expression of adhesion proteins play a role in surface energy related adhesion.

CONCLUSIONS

Efforts to produce directed cell adhesion responses to biomaterial interfaces requires the ability to alter surface characteristics (*e.g.*, surface energy and roughness) for desired cellular proliferation and adhesion. Rather than finding an optimal range of adhesion associated with surface roughness and surface energy, as originally hypothesized, complex trends were observed regarding the relation between surface energy, sur-

face roughness, and fibroblast adhesion. Materials of lower surface energy (*i.e.*, polymers) showed an increase in cellular adhesion strength associated with increased surface roughness, whereas materials of higher surface energy (*i.e.*, metals) demonstrated little change in cellular adhesion strength with increased surface roughness. Overall, surface energy was a more influential surface characteristic than surface roughness on cellular adhesion strength and proliferation. The surface energy components of the various materials tested (HS25, 316L, Ti-6Al-4V, Ta, glass, SR, and PTFE) were shown to be related to cellular adhesion strength. However, the cellular adhesion strength associated with the metallic materials exceeded the cohesion strength of cell membranes. Differences in specific ECM proteins were shown to exist between materials of high and low adhesion strength as well as differences in the general amounts of ECM deposition, with greater amounts of ECM/cell secreted on materials of low adhesion strength (*i.e.*, polymers). TEM observations showed larger gaps between cell and substrate on low-adhesion materials (polymers). Therefore, manipulating surface energy may be a more effective strategy for directing cell adhesion responses, whereas alterations in roughness through microtexturing techniques may be more effective on polymeric surfaces than on inherently highly adhesive metallic biomaterials.

REFERENCES

1. Gristina, A.G. Biomaterial-centered infection; microbial adhesion versus tissue integration. Science **237,** 1588, 1987.
2. Hallab, N., Bundy, K., O'Connor, K., Clark, R., and Moses, R.L. Cell adhesion to biomaterials: correlations between surface charge, surface roughness, adsorbed protein, and cell morphology. J. Long-term Effects Med. Implants **5,** 209, 1995.
3. Hallab, N., Bundy, K., O'Connor, K., Clark, R., and Moses, R.L. Surface charge, biofilm composition and cellular morphology as related to cellular adhesion to biomaterials. Proceedings 14th Southern Biomedical Engineering Conference, Shreveport, LA, pp. 81–84, 1995.
4. Deshpande, M., and Vaishnav, R.W. Submerged laminar jet impingement on a plane. J. Fluid Mech. **114,** 213, 1982.
5. Vaishnav, R.N., Patel, D.J., Atabek, H.B., Deshpande, M.D., Plowman, F., and Vossoughi, J. Determination of the local erosion stress of the canine endothelium using a jet impingement method. J. Biomed. Eng. **105,** 77, 1983.
6. Hallab, N., Bundy, K., O'Connor, K., Clark, R., and Moses, R. Surface charge and energy affect fibroblast adhesion to biomaterials. Trans. 20th Ann. Society for Biomaterials Meeting, New Orleans, LA, 1994.
7. Andrade, J.D., Smith, L.M., and Gregonis, D.E. Contact Angle and Interface Energetics, New York: Plenum Press, 1985.
8. Schakenraad, J.M., Busscher, H.J., Wildevuur, C.R., and Arends, J. The influence of substratum free energy on growth and spreading of human fibroblasts in the presence and absence of serum proteins. J. Biomed. Mater. Res. **20,** 773, 1986.
9. Brash, J.L., and Thibodeau, J.A. Identification of proteins adsorbed from human plasma to glass bead columns: plasmin-induced degradation of adsorbed fibrinogen. J. Biomed. Mater. Res. **20,** 1263, 1986.
10. Merril, C.R., Harasewych, M.G., and Harrington, M.G. Protein Staining and Detection Methods. Bristol: Wright, 1986, pp. 323–362.
11. Moses, R.L. In situ electron microscopy of cultured cells. Bull. Electr. Microsc. Soc. Am. **19,** 60, 1989.
12. Bagnall, R.D. Adsorption of plasma proteins on hydrophobic surfaces. III. Serum, Plasma and whole blood. J. Biomed. Mater. Res. **12,** 707, 1978.
13. Bagnall, R.D., Annis, J.A., and Sherliker, S.J. Adsorption of plasma on hydrophobic surfaces IV. contact angle studies on implanted polymers. J. Biomed. Mater. Res. **18,** 1, 1980.
14. VanDiijk, L.J., Golsweer, R., and Andrade, J.D. Interfacial free energy as a driving force for pellicle formation in the oral cavity: an in-vitro study in beagle dogs. Biofouling **1,** 19, 1988.
15. Sung, K.P., Kwan, M.K., Maldonado, F., and Akeson, W.H. Adhesion strength of human ligament fibroblasts. J. Biomechan. Eng. **116,** 237, 1994.
16. Richards, R.G., Bundy, K.J., Gwynn, I., and Rahn, B.A. Interface connections of fibroblasts with different surfaces after jet impingement testing. In Trans. 10th European Conference on Biomaterials, Davos, Switzerland, 1993.
17. Richards, R.G., Gwynn, I., Bundy, K.J., and Rahn, B.A. Microjet impingement followed by scanning electron microscopy as a qualitative technique to compare cellular adhesion to various biomaterials. J. Cell Biol. Int. **19,** 1015, 1995.

18. Bundy, K., Dillard, J., and Luedemann, R. The use of AC impedance methods to study the corrosion behavior of implant alloys. Biomaterials **14,** 529, 1993.
19. Bundy, K., Rahn, B., Gerber, H., Schlegel, U., Peter, R., and Geret, V. Cell and tissue adhesion to orthopedic biomaterials. In Trans. 39th Orthopedic Research Society, San Francisco, CA, 1993.
20. Bundy, K., Rahn, B., O'Connor, K., Roberts, O., and Gerber, H. Cell adherence to biomaterials of varying surface characteristics. In Trans. 17th Society for Biomaterials, Scottsdale, AZ, 1992.
21. Bundy, K., Rahn, B., Schlegel, U., Geret, V., and Perren, S. Factors affecting soft tissue adhesion to biomaterials. In Trans. 17th Ann. Society for Biomaterials, Scottsdale, AZ, 1991.
22. Kleinman, H.K., Klebe, R.J., and Martin, G.R. Role of collagenous matrices in the adhesion and growth of cells. J. Cell Biol. **88,** 473, 1981.

Address reprint requests to:
Nadim James Hallab, Ph.D.
Department of Orthopedic Surgery
Rush Medical College
1653 W. Congress Parkway
Chicago, IL 60612

E-mail: nhallab@rush.edu